Journal of Cleaner Production 223 (2019) 163–175

Contents lists available at ScienceDirect

Journal of Cleaner Production

journal homepage: www.elsevier.com/locate/jclepro

Experimental study on gas jet suppressed by water mist: A clean control technique in natural gas leakage incidents

Y.P. Liu [a], X.S. Wang [a, *], P. Zhu [a, b], G.C. Li [a], X.M. Ni [a], J. Zhang [a]

[a] State Key Laboratory of Fire Science, University of Science and Technology of China, Hefei 230026, China
[b] Department of Engineering Physics, Tsinghua University, Beijing 100084, China

ARTICLE INFO

Article history:
Received 19 December 2018
Received in revised form
22 February 2019
Accepted 11 March 2019
Available online 15 March 2019

Keywords:
Clean control technique
Natural gas leakage
Water mist
Particle image velocimetry
Flow field

ABSTRACT

Natural gas leakage from gas pipelines usually leads to human intoxication. Further, it may even cause fires and/or explosion accidents or make an indirect chemical contribution to climate change in the long term because of its high global-warming potential. As a clean, potential, and effective method for controlling/mitigating the risk of natural gas leakage, water mist is tested to suppress gas jet leakage from a lab-scale pipe in this study. Based on actual natural gas leakages in pipelines or practical emergency management measures, both tilted and non-tilted gas jet cases were considered to evaluate the performance of gas jet suppression by water mist. A series of small-scale experiments has been conducted to deepen the understanding of the dynamical behavior and mechanisms of the gas jet–water mist interaction by visualizing the two-phase flow via planar particle image velocimetry. The results indicate that different shapes of leakage nozzles with a similar effective diameter are highly consistent regarding the interacting flow field characteristics. In addition, guidelines for optimizing a water mist system for leakage gas suppression/control are presented based on gas–spray momentum ratio and dimensionless gas jet suppression height analyses. Owing to the lack of applications on natural gas leakage with water mist, this study is valuable toward optimizing water mist systems for leakage gas suppression/control of such applications.

© 2019 Elsevier Ltd. All rights reserved.

1. Introduction

Natural gas, as a type of low-carbon clean energy source, has gradually become the main source of energy in most aspects of our society. However, a few concerns regarding the climate implications of natural gas have emerged. On one hand, using natural gas compared with other fossil fuels could be useful in the short term for mitigating climate change. On the other hand, the U.S. oil and gas industry emits 13 million metric tons of methane from its operations each year (Alvarez et al., 2018). The leakage of methane from the production, transportation, and use of natural gas can make an indirect chemical contribution to climate change owing to its higher global warming potential compared with carbon dioxide (Lelieveld et al., 2005; Howarth et al., 2011; Alvarez et al., 2012). Moreover, natural gas leakage accidents, which are mainly caused by pipeline corrosion, equipment aging, and artificial destruction, have become major concerns (Gas Pipeline Incident Data Group, 2014). Once a leak occurs, the leaked high-pressure gas may cause toxic exposure or fire/explosion accidents, resulting in significant casualties and economic losses. Therefore, the development of a clean and efficient method for natural gas leakage prevention/control is important from both scientific significance and practical application perspectives.

Previous studies on controlling and dispersing natural gas leakage focused on dispersing LNG vapor clouds by water curtains. Water curtains are widely used to mitigate LNG vapor because of their availability, economy, and efficiency for gas dispersion, absorption, and fire inhibition (Uzanski and Buchlin, 1998). NFPA 59a (2009) suggests that a water-based fire prevention system will be provided for controlling unignited leaks and spills in LNG facilities. Hald et al. (2005) presented a research methodology involving heavy gas dispersion using water curtains, which involved medium-scale field tests, wind-gallery tests, and numerical simulations. Rana et al. (2008, 2010) conducted a series of LNG spill experiments at the Brayton Fire Training Field at Texas A&M University to study the effectiveness of dispersing LNG vapor clouds by water curtain. Two types of upward directed water curtains were tested, and the full cone type proved to be more effective at

* Corresponding author.
E-mail address: wxs@ustc.edu.cn (X.S. Wang).

https://doi.org/10.1016/j.jclepro.2019.03.107
0959-6526/© 2019 Elsevier Ltd. All rights reserved.

Nomenclature

dt	Interval time between two laser light pulses (μs)
d_e	Effective diameter of leakage nozzle (mm)
D	Gas jet traveling distance from the leakage nozzle to the spray axisymmetric line (mm)
D_p	Diameter of the pipeline (mm)
D_{32}	Sauter mean diameter (mm)
H	Height between the center of gas pipe and gas jet traveling height at the spray axisymmetric line (mm)
H*	Ratio of height of gas jet in the tilt and non-tilt cases under the same gas flow rate
l	Length between centers of semicircle on both sides (mm)
L	Horizontal distance between the center of pipe and spray axisymmetric line (mm)
$\dot{M}_g$	Gas jet momentum (kg m s^{-2})
$\dot{M}_w$	Water mist spray momentum (kg m s^{-2})
$\dot{Q}_{Vg}$	Gas volume flow rate (L min^{-1})
$\dot{Q}_{Mg}$	Gas mass flow rate (kg s^{-1})
r	Radius of leakage nozzle (mm)
S	Area of the leakage nozzle (mm^2)
$u_{g,0}$	Calculated gas jet velocity at the gas jet nozzle exit (m s^{-1})
$u_{w,0}$	Droplet velocity at the water mist nozzle exit (m s^{-1})
Z_g	Height of the gas jet when the average gas jet velocity component in the vertical direction is zero (mm)
Z_{gc}	Critical lift-up distance of the gas jet (mm)
Z_g^*	Normalized lift-up distance of the gas jet
V	Droplet velocity (m s^{-1})

Abbreviations

CCD	Charge-coupled device
CVP	Counter-rotating vortex pair
FoV	Field-of-view
LIP	Laser induced phosphorescence
LNG	Liquefied natural gas
PIV	Particle image velocimetry
PTV	Particle tracking velocimetry
RHP	The ratio of the hole diameter to the pipe diameter

Greek symbols

Φ	Gas–spray momentum ratio
θ_{tilt}	Gas jet tilt angle (°)

controlling the LNG vapor. Compared with traditional water spray systems, water mist has shown a few advantages as a clean and sustainable fire-fighting technique (Zhou et al., 2018, 2019), such as low water consumption and high efficiency for extinguishing fires (Grant et al., 2000; Wang et al., 2002). Zhu et al. (2017) demonstrated that water mist may efficiently suppress/control gas jet leakage involving a small hole based on experiments conducted using a lab-scale natural gas pipeline. They also proposed a correlation to predict the interface position of the downward water mist spray–upward gas jet interaction.

Based on the experimental tests of a downward spray–upward leaked gas jet interaction, it should be noted that in most actual natural gas leakages in pipelines or practical emergency management measures, not only is the water mist system typically applied downward, particularly when using a portable or removable water mist system, but the type of leaking hole is not known, i.e., the gas jet could eject horizontally, vertically, or at any inclined angle from the pipeline. Therefore, there may be cases where the leaked gas jet interacts with the water mist spray flow at an inclined angle, and thus its dynamical processes must be different from those of the downward mist spray–upward gas jet interaction. Furthermore, the capability to control a gas jet leak from a pipeline may be affected by the shape and size of the leak opening.

Thus, in this study, a lab-scale pipeline was used to reproduce gas pipeline leakage and a single 0.5 MPa-water mist spray was also scaled to a relatively low pressure level to reproduce a relatively realistic natural gas leak control process. Nitrogen was selected as leakage gas instead of natural gas owing to safety reasons, such as risk of explosion, fire accident, and poisoning risk. Tilted gas jets with various tilt angles and shapes, and various sizes of the leak opening were taken into consideration. Currently, a few optical measurements can be adopted from related water droplet studies (Volkov et al., 2018; Kuznetsov et al., 2016; Strizhak and Volkov, 2016) for obtaining flow field characteristics such as PIV, PTV, and even LIP. The main goal of this research is to obtain the interaction flow field of the water mist spray and leaked gas jet. PTV is a Lagrangian approach i.e., a technique to measure the velocity of individual particles that are resident in a fluid (Malik et al., 1993), in contrast to PIV, which is an Eulerian method that measures the velocity field of a fluid at a grid. In this study, we focus on the measurement of interaction fields instead of the detailed tracking motion of individual droplets. Thus, the dynamical process of the gas–spray interaction was visualized and analysed based on a 2D-PIV technique, where the water mist droplets were considered as the seeding particles.

The flow field of the gas–spray interaction zone was obtained based on PIV data. The main aim of the research is to obtain the interaction flow field of water mist spray and leaked gas jet, and evaluate the performance of water mist suppression on gas jets through lab-scale experiments including tilted and non-tilted gas jet cases. Owing to the lack of applications on natural gas leakage with water mist, the results of this study provide the gas–spray interaction visualization, and are also valuable toward optimizing water mist systems for leakage gas suppression/control. Further, it helps to develop theoretical modelling on the leakage control by water mist.

2. Experimental setup and measurement techniques

Fig. 1 shows a schematic of the experimental setup. The experimental system can be divided into three subsystems: (1) gas leakage system; (2) water mist system; and (3) flow field diagnosis system, i.e., 2D-PIV system and particle-master shadow system. The experiments were conducted with pure water and nitrogen as working fluids under an ambient room temperature of 20 °C and an atmospheric humidity of approximately 40%. The subsystems will be introduced in the following sections.

2.1. Gas leakage system

Based on the report by the EGIG (Period, 1970–2013) (2014) and research on likelihood, causes, and consequences of leakage incidents in the U.S. natural gas transmission pipelines (Wang and Duncan, 2014), small holes (pinhole/crack) are the primary failure causes among all leakage incidents of transmission pipelines with 4–28 in (i.e., 101.60–711.20 mm) diameter, and account for over

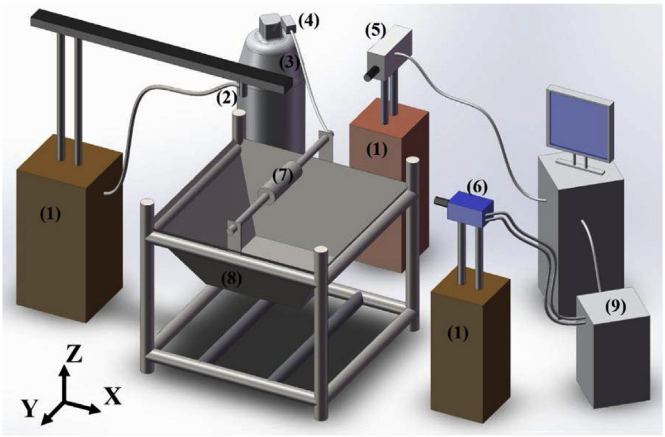

Fig. 1. Schematic of the experimental setup: (1) Optical table; (2) Water mist nozzle; (3) Gas pipeline; (4) Mass flow controller; (5) Nd-YAG laser; (6) CCD camera; (7) Gas jet leakage pipe; (8) Waste-water collection system; (9) Laser controller and data processing system.

50% of all significant incidents. In terms of selection of leakage size, small hole leakage was used to simulate a gas jet release from pipelines. RHP was chosen to characterize the leakage nozzle, which is defined as (Li et al., 2016):

$$RHP = d_e/D_p \quad (1)$$

Where d_e is the effective diameter of the leakage nozzle, which refers to the equivalent diameter of the nozzle and can be expressed as:

$$d_e = \sqrt{4S/\pi} \quad (2)$$

Two types of leakage nozzle shapes: slit leakage and circular leakage nozzles, were adopted in this experiment (as shown in Fig. 2). Real leak situations involving a crack or pinhole are simulated through slit and circular nozzles, respectively.

Because the de of a small hole is less than or equal to 20 mm (EGIG, 2014) and transmission pipelines with 101.60–711.20 mm diameter account for a high frequency of accidents, the nozzle of the gas leakage system was installed at the center of a 400 mm length cylindrical pipe with 40 mm inner diameter. Thus, the RHP of the small hole is less than 0.20 and the effective diameter of the leakage nozzles in this experiment should be scaled to a maximum of 8.00 mm. Six leakage nozzles with various orifice sizes and shapes were tested in this study (shown in Fig. 3). All leakage nozzles and pipelines consisted of 304 stainless steel. In the vicinity of the gas jet nozzle, a MIK-Y180 digital pressure gauge (Hangzhou Asmik Sensors Technology Co., Ltd) was set with ±0.4% full-scale (F.S.) measuring accuracy. Nitrogen (99.99%) was supplied to the cylindrical pipe through the gas supply system and monitored by a CS230A mass flow controller (Beijing Sevenstar Electronics Co., Ltd) with ±1.0% F.S. measuring accuracy.

2.2. Water mist system

A nozzle with a 1.0 mm orifice was installed 550 mm above the top surface of the gas pipe, which adopted the pressure swirl atomization method and could produce a full-cone spray. The water spray was driven by a high-pressure pump and monitored by a pressure gauge with ±1.6% F.S. measuring accuracy (China Hongqi Instrument Co., Ltd). The water mist working pressure was fixed at 0.5 MPa in all experiments. Based on NFPA 750 (2010), a low-pressure system where the distribution piping is exposed to pressures of 12.1 bar or less was applied in this experimental study.

Fig. 4 shows details of the water mist nozzle structure and its spray pattern captured by a CCD camera. A 68° spray angle was measured by the photo of the water mist spray illuminated by a laser sheet under 0.5 MPa working pressure. The flow discharge coefficient of the nozzle is 0.35 L min^{-1} MPa and the details of the water mist characteristics are presented in Section 3.1.

2.3. Flow field diagnosis system

In 2D-PIV measurement, the displacement of particles in the time between the laser pulses is recorded as a pair of two single exposure images, i.e., double frame/double exposure. The recorded particle displacement field is measured locally across the whole field of view of the images, scaled by the image magnification and then divided by the known pulse separation to obtain flow velocity at each point (FlowMaster, 2015). The setup of 2D-PIV system was also presented in Fig. 1. A double-pulsed Nd:YAG laser with a 200 mJ/pulse, 532 nm wavelength and 14.73 Hz repetition rate was used to illuminate the interaction filed. A CCD camera (LaVision Imager ProX2M) with the resolution of 1600 × 1200 pixels and pixel size of 7.4 × 7.4 μm positioned typically perpendicular to the plane of the laser sheet is used to capture the light scattered from the water mist droplets. In the image acquisition and interrogation of PIV recording, the PIV recording is divided in small subareas (i.e. interrogation windows) and 32 × 32 pixels of interrogation windows size was used to capture all droplets particles within the interrogation cell for vector processing. In order to obtain accurate flow field vector information, d**t,** the interval time between two laser light pulses must be optimized. According to previous works on optimization of PIV (Keane and Adrian., 1990; Adrian and

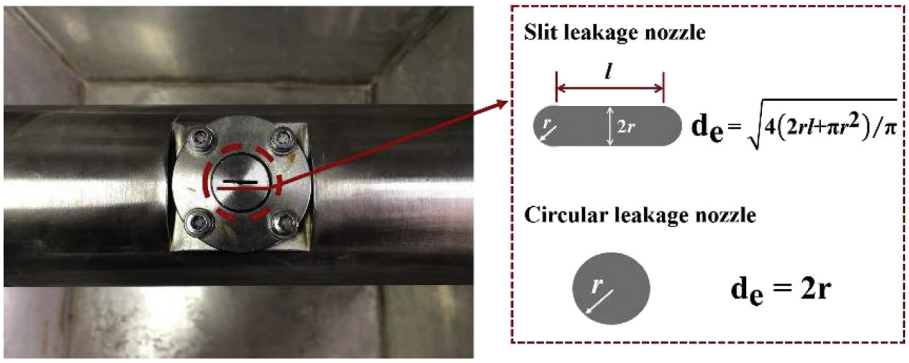

Fig. 2. Schematics of two types of leakage nozzles.

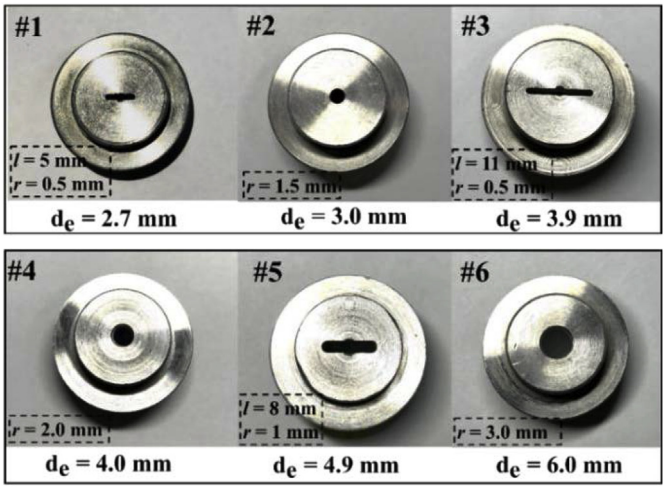

Fig. 3. Details of the six leakage nozzles.

Westerweel., 2011) and recommendations offered by Lavison (FlowMaster, 2015), the maximum velocity particle displacement in a measurement area with 5–8 pixels is relatively suitable. Husted et al. (2009) conducted a series of PIV droplet velocity measurement with the average pixel movement of 4–8 pixels under high-pressure (i.e. 100 bar) water mist nozzles. Thus all the selections of d**t** satisfy the average pixel movement of 4–8 pixels in this study. In the post-processing of PIV data, cross correlation with multi-pass iterations was applied for improving the signal-to-noise and accuracy in vector calculation.

In the 2D-PIV tests, owing to the limitation of using a single CCD camera, the same case was tested four times to obtain a full view of the field using four sub fields of the view, where each sub field was 196.89 mm × 147.67 mm with approximately 0.12 mm/pixel spatial resolution. A water mist nozzle was mounted at 0 mm (measuring error among all tests: 0–7 mm) above the upper part of FoV 04, and the bottom of FoV 01 was flush with the upper surface of the gas jet leakage pipe. The centers of all sub fields of view and the nozzle position are on the same vertical axis, as shown in Fig. 5. Different sub field measurements were conducted at different times in the same experiment cases; therefore, the final reconstructed results of the flow field contain a few limitations. However, the results show that the combination of the sub view field velocity vectors has sufficient continuity.

Regarding the choice of seeding particles, Melling (1997) discussed the size specifications for suitable seeding particles for PIV by focusing on the flow tracking capability. The selection of the seeding particles was a compromise between an adequate tracer response of the small-diameter particles in the fluid and a high signal-to-noise ratio of the scattered light signal with the large-diameter particles. On the reliability of flow field measurements with water mist droplets as the seeding particles, numerous studies have validated that the Sauter mean diameter of up to 100 μm is practical for experiments with PIV measurements (Husted, 2007; Husted et al., 2009; Santangelo, 2010). Thus the droplets generated by water mist nozzle are directly used for seeding particles. The leaked gas jet has not been seeded in this experiment.

Particle-master shadow system was applied to measurement of water mist droplet size. Particle-master shadow features a double-pulsed 532 nm Nd-YAG laser, programmable timing unit, LaVision diffuser with a 120 mm output aperture, mirror-based long distance microscope, which has a working range of 560 mm–1520 mm and 70 mm back focal length, a CCD with an *f*-number between 8.7 and 16.8, and LaVision computer with DaVis 8.3 software. The laser pulse energy was adjusted to 100 mJ to avoid damage to the CCD camera by a high-optical density incidence. The pulse width (5–10 ns) and interval between the pulses were programmed by the DaVis 8.3 software according to the desired application. The Particle-master shadow system setup and apparatus arrangement were detailed in our research group works (Wang et al., 2018).

2.4. Experimental conditions and procedure

Different configurations and orientations of leakage nozzles are considered in the experiments. In terms of experiment case design, two types of orientations, including tilted cases and non-tilted cases, were chosen. In tilted cases, two leakage nozzles with six tilt angles were tested under 0.5 MPa pressure water mist spray. Fig. 6(a) shows the arrangement of tilted cases, where D is the gas jet traveling distance from the leakage nozzle to the spray axisymmetric line and L is the horizontal distance between the center of the pipe and the spray's axisymmetric line. In the tilted experimental cases, variation of both the tilt angle, θ_{tilt} and the gas jet separation distance D from the leakage nozzle to the spray axisymmetric line were considered. That is, hold the tilt angle constant and vary the distance D, then separately, hold constant the

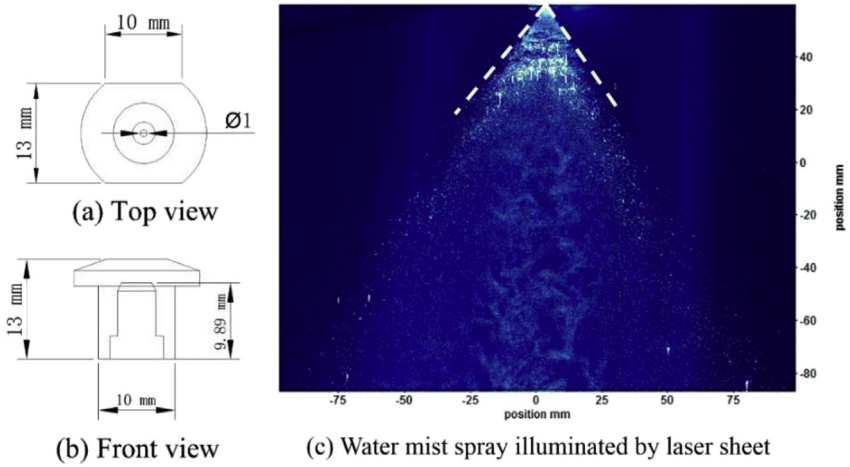

Fig. 4. Sketch of the water mist nozzle and its spray pattern.

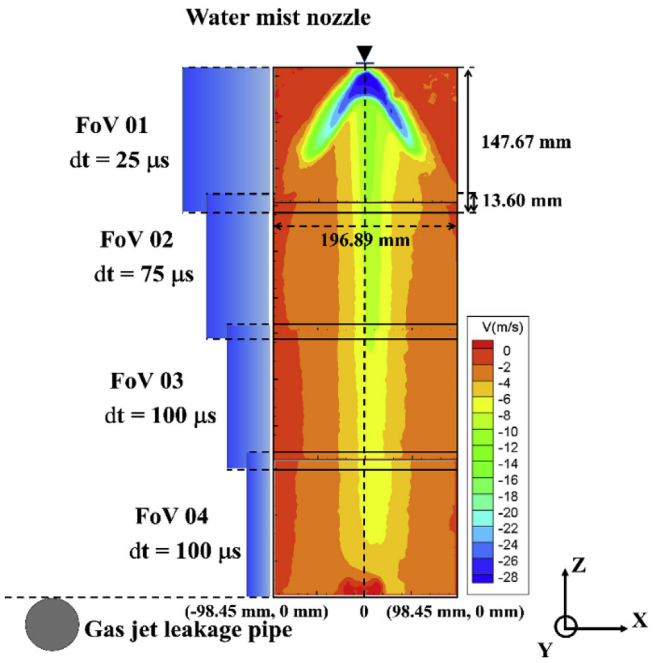

Fig. 5. Layout of the combined FoVs and corresponding d**t** values.

distance D and vary the tilt angle. Results from this wider array of test conditions should be significantly more relevant to actual leakage scenarios. Two leaks with nozzle #3 and nozzle #4 were conducted for these cases, which were used to evaluate the dynamics and capability of gas leakage control using a water mist spray under the same tilted conditions for nozzles with basically the same effective diameter. In the non-tilted experimental cases, the gas jet interacts directly with the water mist spray in the vertical direction, as shown in Fig. 6(b). Zhu et al. (2017) conducted a series of non-tilted experiments with a 2 mm circular leakage nozzle under a similar experimental setup, but did not consider different nozzle types. Therefore, in our non-tilted experimental cases, leakage tests involving various shapes and sizes of nozzles (see Fig. 3) were conducted to investigate the influence of leakage configurations on control of a gas jet from a small hole leak.

Table 1 presents the experimental cases and corresponding parameters. All experiments were conducted under a 0.5 MPa-working pressure water mist system and the nozzle installation height was fixed at 550 mm. If L is too close to the spray axisymmetric line, the gas jet will interact with only half of the water mist spray and it is difficult for the CCD to capture the full interaction zone owing to the CCD's fixed position. Thus setting L > 50 mm was determined by pre-tests. With the height of the nozzle fixed at 550 mm and L > 50 mm, the maximum H is 500 mm and the minimum H is 50 mm. Thus, a reasonable value of D with varying θ_{tilt} was obtained by setting H = 50–500 mm and L > 50 mm to better capture the interaction flow field in the FoV.

According to the small hole model for accidental release (Dong et al., 2002; Jo and Ahn, 2003), the gas jet velocity at the leakage nozzle ($u_{g,0}$) can be identified. The detailed calculation of the velocity is presented by Zhu et al. (2017). Table 2 lists the gas jet velocities at the leakage nozzle for all cases.

The detailed experimental procedure is shown in Fig. 7. To eliminate the background light effects on PIV imaging, the entire workplace was enclosed by black cloth curtains to achieve dark-room conditions. Detecting the gas leakage in pipelines is a necessary procedure in real leakage incidents. In engineering applications, automated detection (e.g., fiber optic or cable sensors), semi-automated detection (e.g., statistical or digital signal processing methods), and manual detection (e.g., thermal imagers or LIDAR devices), which depend on the degree of human intervention required, are applied (Murvay and Silea, 2012). In our experiments, the gas jet was activated prior to water mist injection during each test. Once we activated the gas leakage system, the water mist spray was then released.

2.5. Uncertainty analysis

The overall measurement uncertainty of two-phase flows using 2D-PIV is comprised of systematic and random uncertainties. Uncertainties arise from numerous uncertainty sources, which include the experimental setup, PIV processing, and stochastic nature of two-phase flows. To some extent, the setup of the measurement sub views and combined flow field eliminated the errors by moving the CCD camera to obtain each sub view. Random deviation

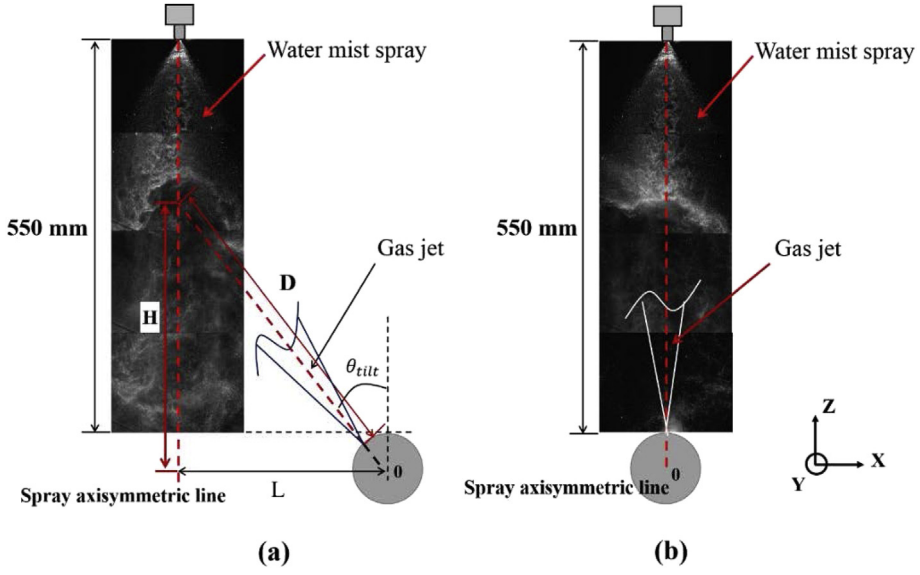

Fig. 6. Schematic of the mist spray–gas jet interaction: (a) tilted cases; (b) non-tilted cases.

Table 1
Experimental cases.

Case number	Leakage nozzle	$\dot{Q}_{Vg}$ (L min^{-1})	θ_{tilt} (°)	D (mm)
Non-tilt-01	#1	30/50/70/90	0	–
Non-tilt-02	#2	30/50/70/90	0	–
Non-tilt-03	#3	30/50/70/90	0	–
Non-tilt-04	#4	30/50/70/90	0	–
Non-tilt-05	#5	30/50/70/90	0	–
Non-tilt-06	#6	30/50/70/90	0	–
Tilt-01	#3/#4	30/50/70/90	15	260/360/460
Tilt-02	#3/#4	30/50/70/90	25	160/260/360/460
Tilt-02	#3/#4	30/50/70/90	35	160/260/360/460
Tilt-04	#3/#4	30/50/70/90	45	160/260/360/460
Tilt-05	#3/#4	30/50/70/90	55	160/260/360
Tilt-06	#3/#4	30/50/70/90	65	160/260/360

sampling of the statistical errors can be avoided by performing numerous individual and repeated measurements (Westerweel, 2000). The stochastic nature of two-phase flows is generally a result of the physical and optical interference caused by bubbles. In the experimental scenario of the interaction between a water mist spray and gas jet, significant production of bubbles is difficult, and therefore, this type of effect on the PIV measurements can be neglected.

According to the PIV measurements on water mist performed by Husted et al. (2009), the random variation in the measured mean velocities caused by random errors was estimated to be 5% of the instantaneous velocity measurement for all components, based on a 95% confidence level. The influence of fixed errors was difficult to determine, thus, an attempt was made to directly estimate the total error from repetitive measurements. This resulted in an estimated total error in the mean velocities of approximately 10%. Owing to the similarity of the full cone water mist spray using the same model of LaVision PIV system used in Husted et al. (2009) study, a total error of 10% was applied to the mean velocities in our study.

Owing to the physical property differences between nitrogen and natural gas, there is an inevitable difference in gas dynamical properties, such as velocity and momentum. Thus, there is a limitation in our experimental results because nitrogen was used as a substitute for natural gas for safety reasons.

3. Experimental results and discussion

A series of lab-scale experiments for controlling/suppressing leakage gas jets by low-pressure water mist spray were conducted. The gas–spray interaction flow field characteristics and water mist characteristics were obtained from flow field diagnosis system. An analysis based on the gas–spray momentum ratio was carried out and a dimensionless height was used to evaluate the control capabilities of water mist between tilted and non-tilted leakage cases.

3.1. Water mist characteristics

Regarding water mist system application, a few important characteristics, such as the mist flux density distribution, droplet size, and velocity should be characterized. They are also the effective parameters for evaluating the dynamic behavior of a water spray interacting with a leaked gas jet.

Table 2
Details of gas jets for all cases.

Leakage nozzle	$\dot{Q}_{Vg}$ (L min^{-1})	$u_{g,0}$ (m s^{-1})
#1	30/50/70/90	89.80/141.42/186.43/233.58
#2	30/50/70/90	80.56/141.42/179.45/218.94
#3	30/50/70/90	57.32/80.57/105.62/130.84
#4	30/50/70/90	57.32/80.57/98.08/125.12
#5	30/50/70/90	40.66/57.32/80.57/89.80
#6	30/50/70/90	40.66/40.66/57.32/69.99

3.1.1. Water mist flux density distribution

The distribution of the water mist flux density was measured by a collection method, i.e., by placing a water collection tray of dimensions 0.593 m × 0.593 m × 0.1 m consisting of 144 circular tubes (with 4.2 cm diameter and 8 cm depth) 550 mm beneath the water mist nozzle. Fig. 8 shows the water mist flux density distribution under 0.5 MPa working pressure. It can be observed that the densest flux density is concentrated in the center area and that the flux density decreases along the radial direction.

3.1.2. Water mist droplet size and velocity

Shadowgraph technology was adopted to measure the size of the water mist droplets using the LaVision particle-master system before their interaction with the leaked gas jet. An imaging field of approximately 6.33 × 4.75 mm^2 was viewed to capture the droplets, and the spatial resolution was approximately 3.96 μm/pixel. In general, D_{32}, the Sauter mean diameter, is used to characterize the droplet size of water mist spray. Therefore, Fig. 9 presents the droplet size with $D_{32} = 54$ μm at 550 mm below the 0.5 MPa-pressure water mist. A total of 300 experimental image pairs (20.3s@14.73Hz) were recorded to obtain the average droplet size in the measurement field.

The PIV technique was adopted to measure the velocity of the water mist droplets. A few typical droplet velocities in FoV 01 with $\mathbf{dt} = 25$ μs are shown in Fig. 10. The results of droplet velocity at

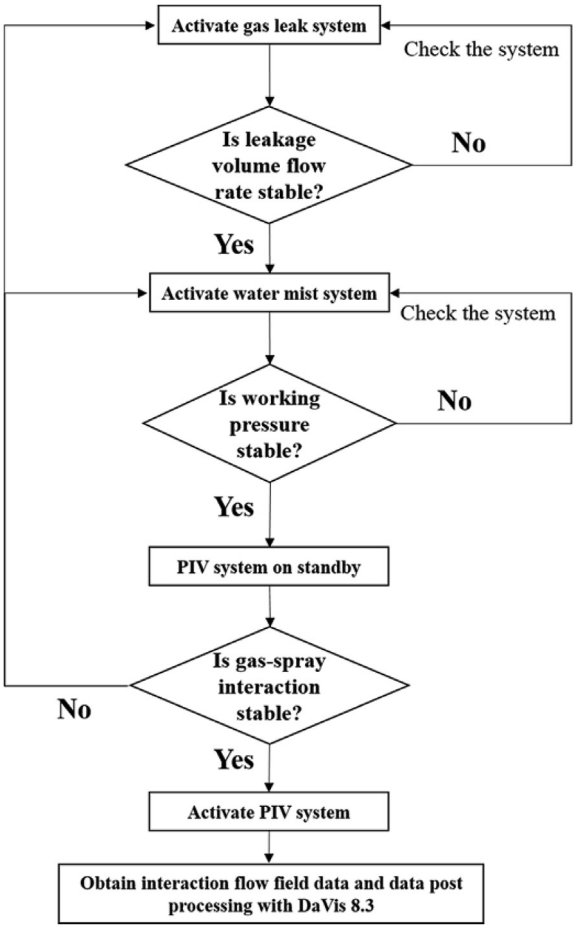

Fig. 7. Flowchart of experimental procedure.

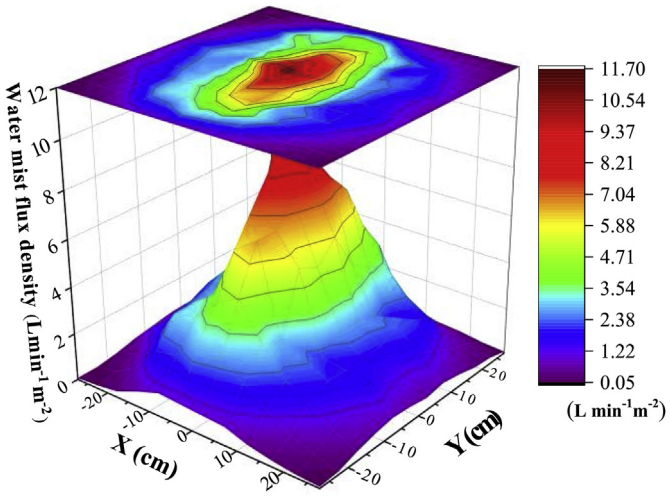

Fig. 8. Color map surface projecting water flux density distribution. (For interpretation of the references to colour in this figure legend, the reader is referred to the Web version of this article.)

20 mm, 30 mm, 40 mm, and 50 mm beneath the 0.5 MPa-pressure water mist nozzle indicate that: (1) the droplet velocity initially increased and then decreased along the radial direction; (2) the droplet velocity tended to decrease around the centerline of the water mist spray with longer separation distance from the water mist nozzle; (3) the droplet velocity could be generally characterized as having a 2D-symmetrical distribution. The maximum of the droplet velocity was considered as the initial droplet velocity at the nozzle in Section 3.2.2.

3.2. Interaction of non-tilted gas jet and water mist spray

In this section, six different leakage nozzles were used to evaluate the effect of the leak size and shape on water mist suppression/control of a non-tilted gas jet. A few typical droplet flow characteristics and quantitative analysis based on the kinetics of the interacting flow field were obtained.

3.2.1. Interaction flow field

The interaction of the gas jet and water mist spray was captured and the interaction flow field in FoVs 01–04 was obtained by the 2D-PIV system. In post processing, the time-averaged flow patterns of the velocity and streamlines were determined from 100 recorded image pairs (6.79s@14.73Hz). Fig. 11 shows the time-averaged flow field of all non-tilted cases, and the typical interaction region in the gas–spray boundary is displayed in the corresponding FoV.

For the relatively low gas flow rates (for example, 30 $Lmin^{-1}$ and 50 $Lmin^{-1}$) illustrated in Fig. 11, a clear gas–spray interaction interface was not formed in all cases based on the measurement results. By increasing the effective diameter of the leakage nozzle, the gas jet is suppressed near the leakage nozzle and the suppression performance is better for the larger leakage nozzles. For the cases with relatively larger gas flow rates of 70 and 90 $Lmin^{-1}$, a CVP is produced, owing to the more intense interaction between the gas flow and water mist spray flow, which causes air to become entrained, and droplets are drawn/sucked into the entrained air. With decreasing leakage size, the gas–spray interface moves up and vortices are formed. For instance, the gas–spray interface was evidently lifted from FoV 04 to FoV 02. Thus, the results of the interaction flow field illustrate the effects of the leakage size and shape on water mist suppression/control of non-tilted gas jets.

3.2.2. Analysis based on gas–spray momentum ratio

In multiphase studies, the gas-to-liquid momentum ratio is a common parameter used to characterize the interactions in gas–liquid two-phase flows. The jet-to-crossflow momentum flux ratio has been widely adopted in studies of a liquid jet in a gaseous crossflow (Broumand and Birouk, 2016). Nam (1996) and Schwille and Lueptow (2006) discussed the interaction between a sprinkler spray and fire plume in terms of the momentum ratio between the upward fire plume and downward spray. Therefore, the gas–spray momentum ratio was adopted in this study. The gas–spray momentum ratio Φ was redefined to consider the tilt

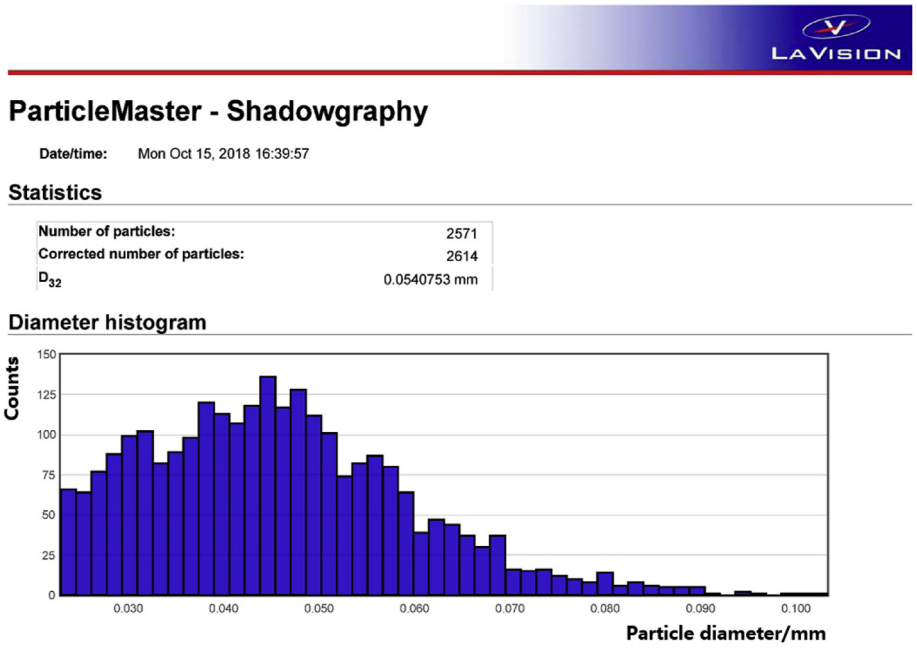

Fig. 9. Shadowgraphy report of droplet sizes by the LaVision particle-master system.

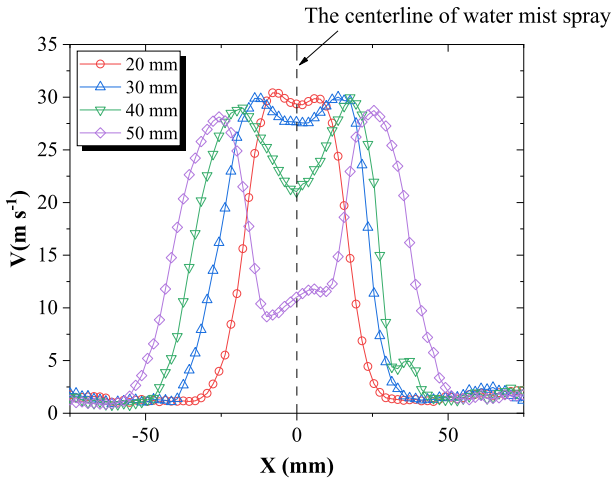

Fig. 10. Droplet velocity along radial distribution at 20 mm, 30 mm, 40 mm, and 50 mm below the 0.5 MPa-pressure water mist nozzle.

angle θ_{tilt}. To characterize the gas–spray momentum ratio for the different tilted gas jet cases, the gas jet flow momentum was decomposed into horizontal and vertical components. The gas–spray momentum ratio Φ essentially reflects the competition between the water mist spray and the gas jet in the vertical direction. Therefore, the ratio of the gas–spray momentum in this experiment that includes the tilt angle can be defined as

$$\Phi = \left(\dot{M}_g \cos(\theta_{tilt})\right) \Big/ \dot{M}_w \tag{3}$$

The gas jet momentum was calculated based on the initial gas momentum at the leakage nozzle exit as

$$\dot{M}_g = \dot{Q}_{Mg} u_{g0} \tag{4}$$

$$\dot{M}_w = \dot{Q}_{Mw} u_{w0} \tag{5}$$

where u_{w0} (m s^{-1}) is the droplet velocity at the water mist nozzle exit. The maximum axial velocity obtained from the measured results in FoV 01 was approximated as the initial droplet velocity near the nozzle exit.

Fig. 12 shows the schematic of the Z_g calculation process, where Z_g refers to the height of the gas jet when the average gas jet velocity component in the vertical direction is zero, as obtained from the time-averaged flow field. Therefore, the height of the gas–spray interaction interface is determined by the value of Z_g in this experiment.

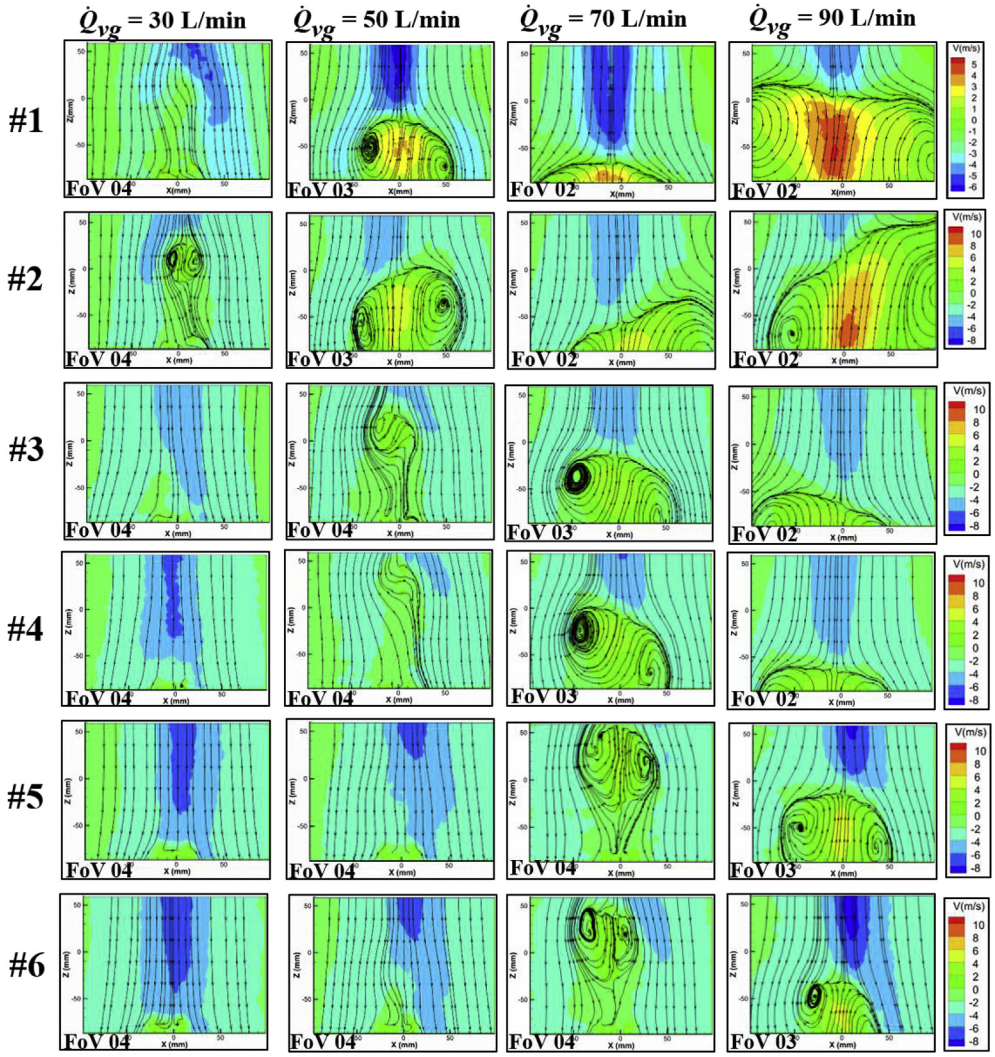

Fig. 11. Time-averaged flow field of the interaction regions at the gas–spray boundary in the non-tilted case.

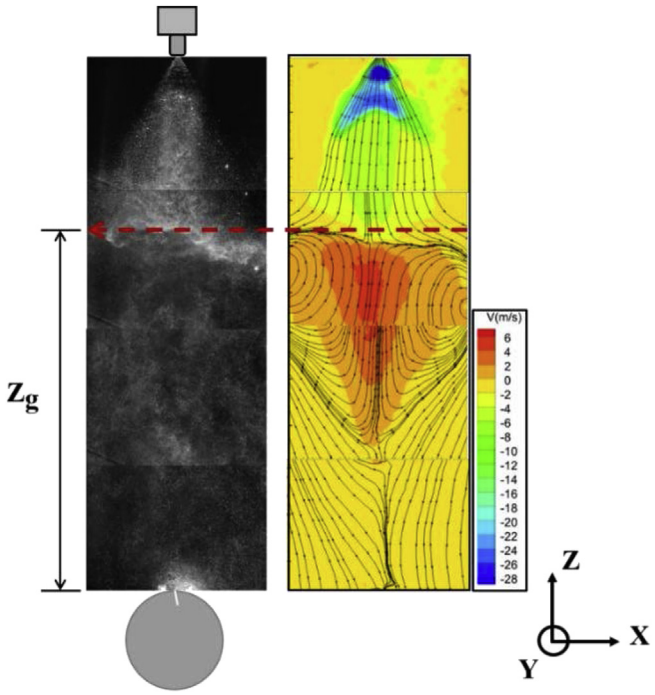

Fig. 12. Schematic of Z_g calculation process and typical flow visualization with corresponding flow field in the non-tilted case.

The normalized lift-up distance is $Z_g^* = Z_g/Z_{gc}$ ($Z_{gc} = 275$ mm) and is considered along with the gas–spray momentum ratio, Φ. The definition of the normalized lift-up distance and value of critical lift-up distance of the gas jet are adopted from the work of Zhu et al. (2017). Z_g^* is an important parameter for evaluating the performance of water mist suppressing a gas jet. In the gas–spray interaction, the normalized lift-up distance can represent the diffusion propagation properties of a gas jet in the water mist spray. In this study, the gas jet is well suppressed by water mist when $Z_g^* < 1$ and further design of a water mist system should be considered when $Z_g^* > 1$.

Fig. 13 shows that the values of Z_g^* and Φ for all non-tilted cases. With an increase of the effective diameter of the leakage nozzle, the height of the gas–spray interaction interface exhibits a downward trend. It is worth mentioning that leakage nozzles #3 and #4, with a similar effective diameter and different leak shapes, basically have the same Z_g value under the various gas flow rates. Leakage nozzles #5 and #6, with a larger effective diameter, also basically have the same Z_g under the various gas flow rates. The lines for $Z_g^* = 1$ and $\Phi = 1$ divide the complete figure into four sub regions, where the region for $Z_g^* > 1$ and $\Phi < 1$ indicates that the gas jet is not well suppressed by the mist spray. It is clearly shown that water mist spray does not have the capability to suppress a gas jet leak when the effective diameter of the leakage nozzle is less than 4 mm. The region for $Z_g^* > 1$ and $\Phi > 1$ also indicates that the gas jet was not well suppressed by the water mist spray in this experiment. The cases of leakage nozzles with $d_e \leq 3.0$ mm, and where $\dot{Q}_{Vg} \geq 90$ Lmin^{-1}, should be of particular note in leakage incidents. Thus engineers should improve the performance of the water mist, i.e., by increasing its initial spray momentum, in these cases.

Fig. 13(b) shows that the values of Z_g^* and Φ for all the non-tilt cases can be strongly correlated by an exponential fitting function ($Z_g^* = 1.68 - 1.92e^{(-1.88\Phi)}$). Thus it can be concluded that analysis based on gas–spray momentum ratio can well cover the different leak types in small hole leakage type incidents. For practical engineering applications, an empirical statistical prediction correlation can be used to obtain a rough estimate of the normalized gas jet lift-up distance.

3.3. Interactions between tilted gas jet and water mist spray

In this section, leakage nozzles #3 (slit) and #4 (circular) with a similar effective diameter were used to evaluate the effect of water mist control of tilted gas jets. By varying the tilt angle θ_{tilt} and the distance D, the flow field characteristics, a few quantitative analyses based on Φ, and a comparative analysis with non-tilted cases are discussed.

3.3.1. Interaction flow field

Fig. 14 shows the schematic of the Z_g calculation process, where Z_g refers to the height of the gas jet and titled leakage nozzle when the average gas jet velocity component in the vertical direction is zero, as obtained from the time-averaged flow field. Compared with non-tilted cases, a single vortex in the gas–spray interaction interface was formed instead of a CVP (see Fig. 15), which indicates a relatively strong gas-droplet mixing area, where the downward droplets interact with the tilted gas jet flow at a relative high velocity, and where a portion of the droplets were sucked into the gas flow.

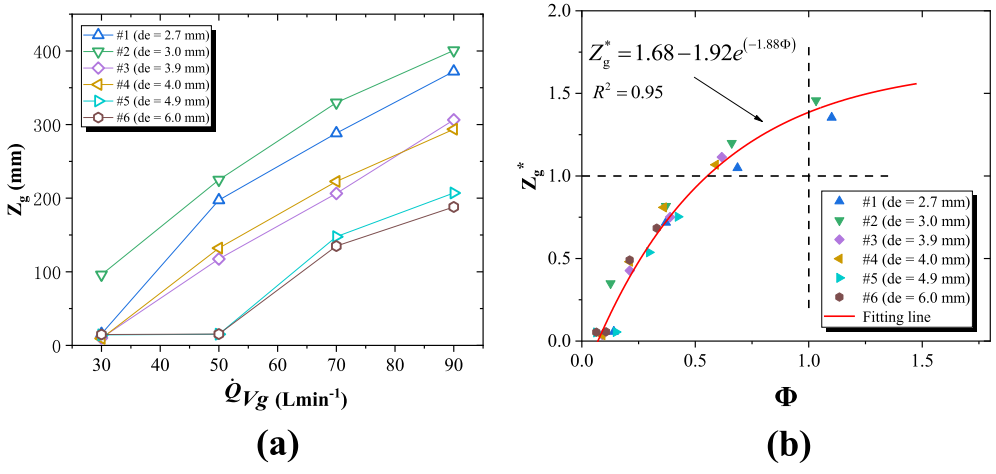

Fig. 13. Gas jet height and normalized lift-up distance versus gas–spray momentum ratio for all non-tilted cases.

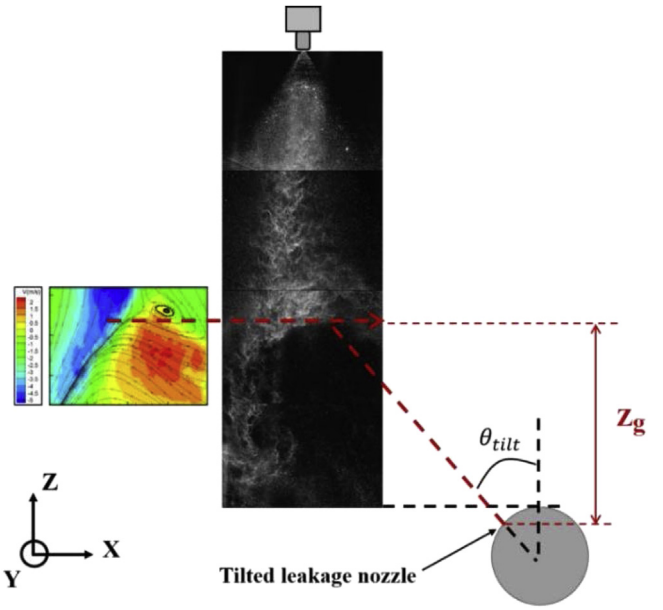

Fig. 14. Schematic of Z_g calculation process and typical flow visualization with corresponding flow field in tilted case.

In terms of droplet motion, the downward droplets in the +X direction were entrained in the tilted gas jet flow. When the momentum of the gas jet is relatively high, the entrained droplets then are lifted upward and impinge on the downward droplets in the −X direction, and then gradually converge into downward droplets. Thus, a tilt gas–spray interface was formed in a few cases (see the cases with D = 360 mm in Fig. 16(a)) In other cases, not all droplets gradually converged into downward droplets and relatively low velocity droplets interacted with downward droplets, leading to a gas–spray mixing vortex in the −X direction (see Fig. 15).

As an example of a typical flow field feature analysis, the entire series of time-averaged flow field diagrams in tilted cases with 90 $Lmin^{-1}$ gas flow rate are displayed in Fig. 16. With the increase of D at the same tilt angle, the gas–spray interaction interface gradually lifted. For a relatively shorter D, the vortex structure was not formed, and gas flow was dominated by the downward spray. As the tilt angle increased at the same D, the height of the gas–spray

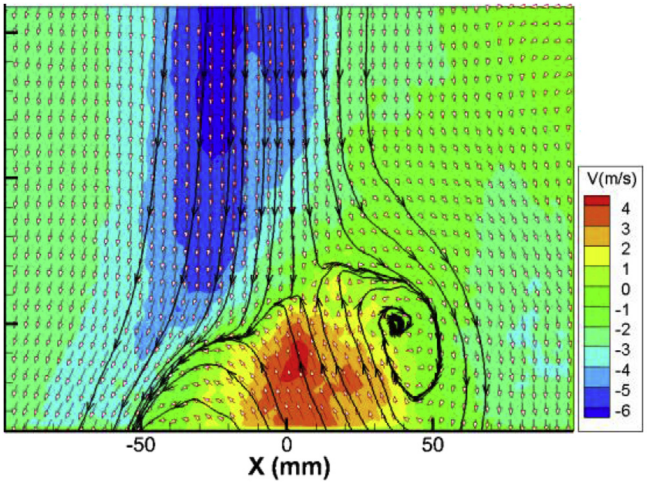

Fig. 15. Typical interaction flow field with vector and streamlines for $\theta_{tilt} = 15°$, D = 460 mm, and 90 L min^{-1} gas flow rate in FoV 02.

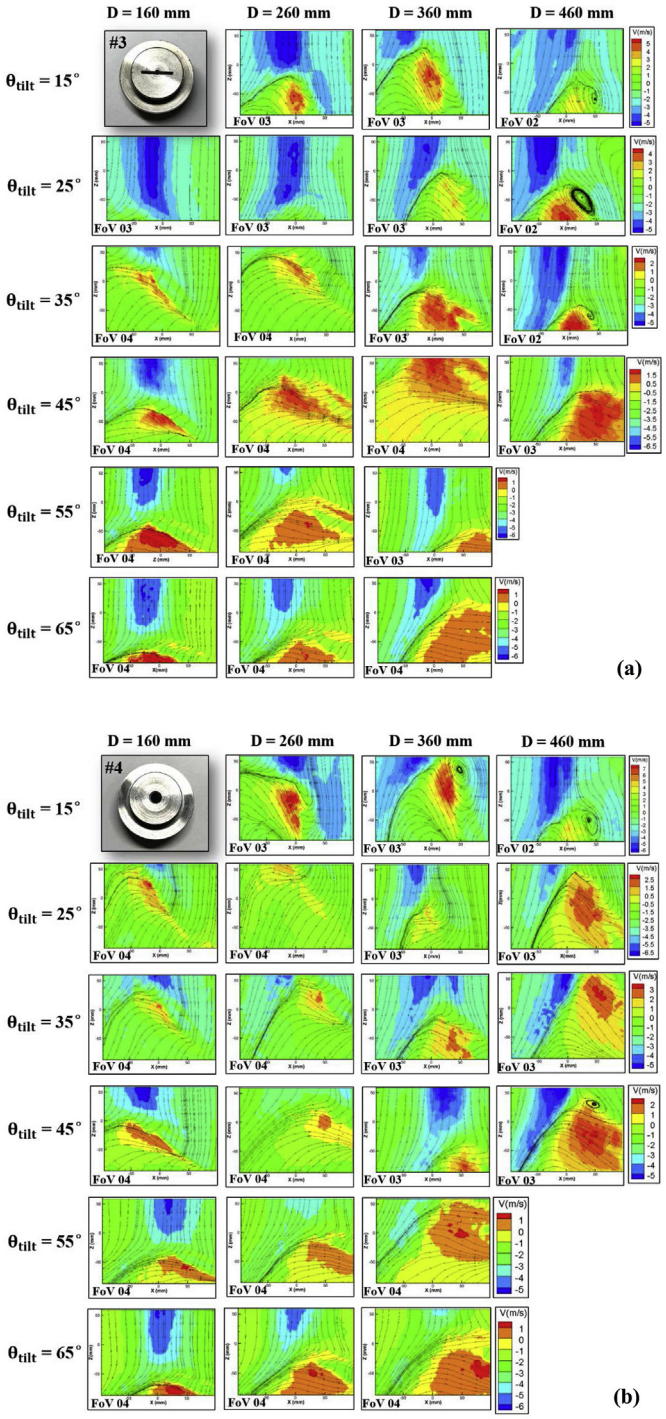

Fig. 16. Time-averaged flow field of the interaction region with gas–spray boundary under the cases with tilted gas jet flow of Q_{Vg} = 90 $Lmin^{-1}$: (a) leakage nozzle #3 cases; (b) leakage nozzle #4 cases.

interaction interface gradually decreased owing to the smaller gas–spray momentum ratio in the vertical direction. Thus, the vortex structure was only found in relatively low tilt angle cases.

3.3.2. Comparative analysis

For better comparison with the results of non-tilted conditions, a dimensionless height H^* is defined as the ratio of Z_g in the tilt cases and non-tilt cases under the same gas flow rate, i.e., $H^* = Z_g$ (tilt)/Z_g (non-tilt). Water mist spray has a better suppression effect

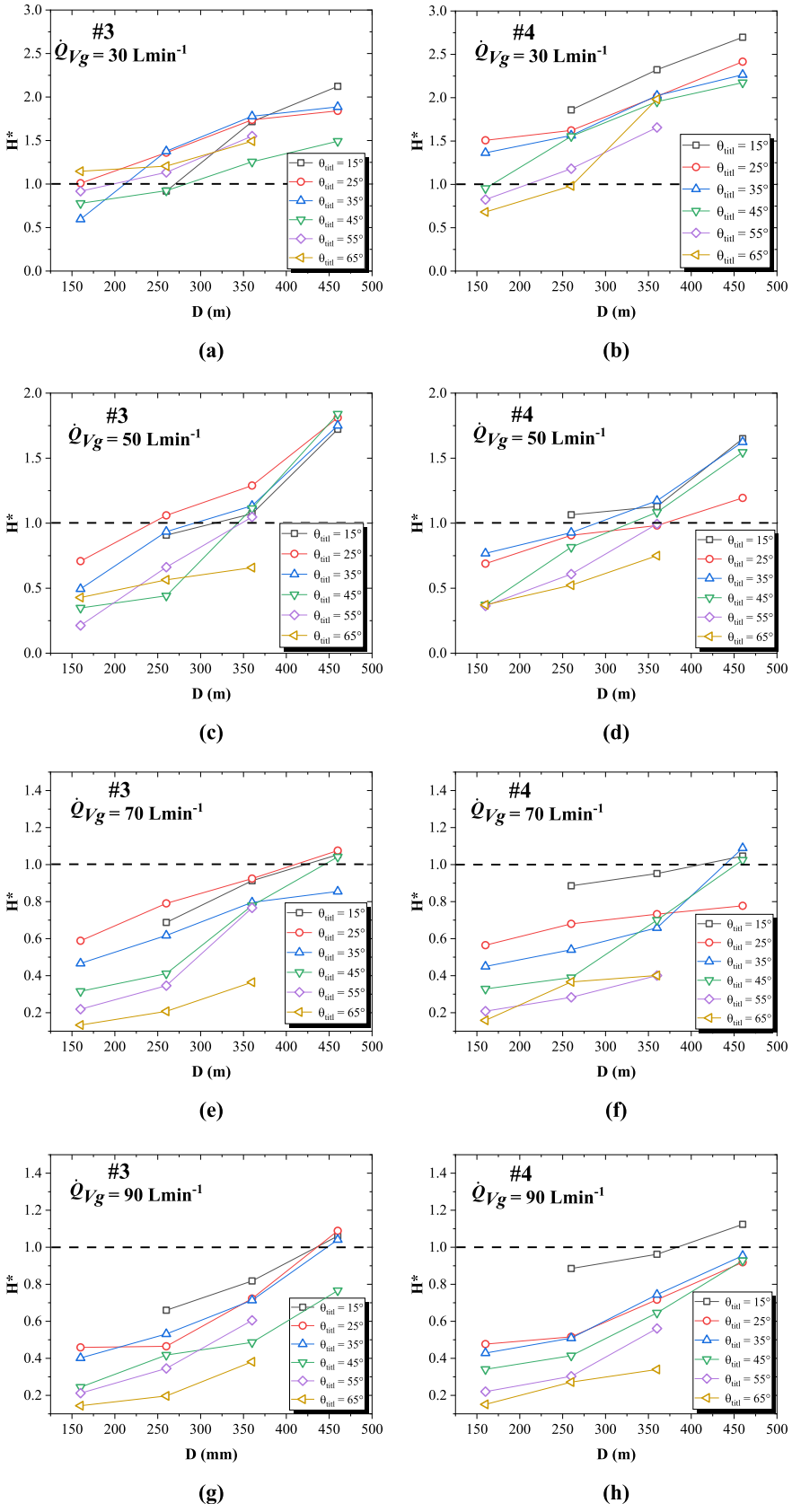

Fig. 17. Dimensionless height H* versus D under different tilt angles and gas flow rates for leakage nozzles #3 and #4.

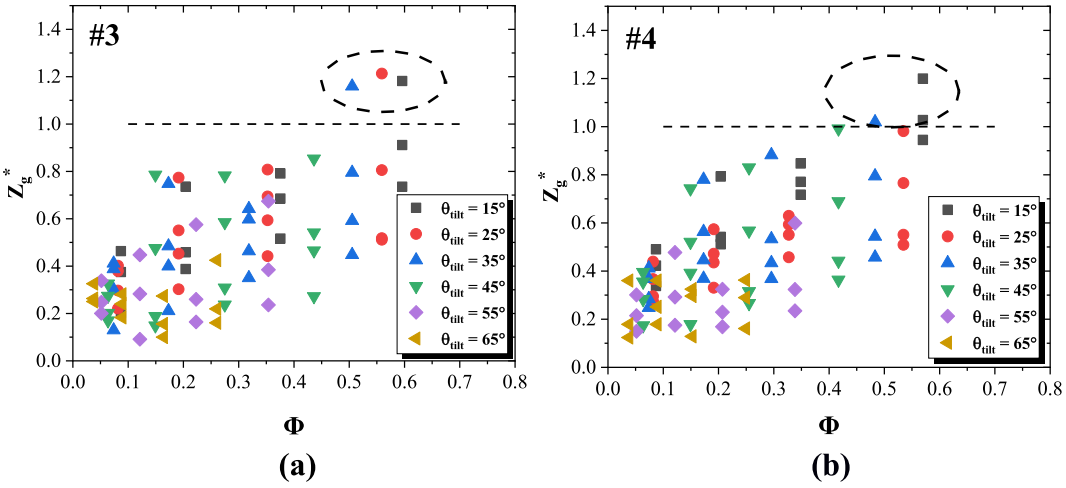

Fig. 18. Normalized lift-up distance versus gas–spray momentum ratio for all tilted cases.

on tilted leaks when the dimensionless height H* is less than 1, as indicated by Fig. 17. A few conclusions can be drawn from Fig. 17 as follows: (1) as the leaked gas flow rate increases, the height of the gas–spray interaction zones with the tilted gas jet gradually decrease below those of non-tilt cases, and thus, water mist spray has a significantly better suppression effect on tilt cases, in particular, when the gas flow rate is greater than 50 Lmin^{-1}; (2) In cases involving the same tilt angle, water mist spray exhibits poor suppression capability compared with non-tilt cases with increases of D; (3) The dynamics of gas–spray interactions of different shapes but with the same leakage size are highly consistent in both tilt and non-tilt cases.

Fig. 18 presents all results of the tilted cases based on gas–spray momentum ratios. The cases with $\dot{Q}_{Vg} = 90$ Lmin^{-1} and D = 460 mm produce the highest gas–spray interaction interface in the respective tilt cases. Although the tilted gas jet momentum on a vertical component is less than in a non-tilted case for the same gas flow rate, the region of $Z_g^* > 1$ includes certain tilted cases. The cases when $\theta_{tilt} \leq 35°$, D ≥ 460 mm and $\dot{Q}_{Vg} \geq 90$ Lmin^{-1} can be considered as a critical condition to determine whether an enhanced water mist system must be activated (see black dotted circle in Fig. 18) in tilt cases.

4. Conclusions

Lab-scale experiments for controlling/suppressing leakage gas jets by low-pressure water mist spray were conducted to reproduce a relatively realistic natural gas leak disposal process. The main conclusions drawn from this study can be summarized as follows:

(1) Leakage nozzles with a similar effective diameter but different leak shapes, basically have the same gas jet height under various gas flow rates. Otherwise the gas–spray interaction zone lifted up with decreasing effective nozzle diameter, which indicates that effective nozzle diameter can be considered as a good means to characterize leakage size, both in crack and circular leak incidents.

(2) An empirical statistical prediction correlation $Z_g^* = 1.68 - 1.92e^{(-1.88\Phi)}$ based on normalized lift-up distance and gas–spray momentum ratio analyses, was derived to provide a rough estimate of the normalized gas jet lift-up distance in non-tilted cases. Thus, the gas–spray momentum ratio can well cover the different leak shapes in small hole leakage type incidents when evaluating water mist spray system requirements.

(3) Comparative analysis evaluating the performance of water mist in non-tilted and tilted leaked gas situations was discussed via the H* parameter. As the leaked gas flow rate increases, the height of the gas–spray interaction for a tilted gas jet gradually decreases below the non-tilt cases, and water mist spray has a significantly better suppression effect on tilt cases, in particular, when the gas flow rate is greater than 50 L min^{-1}.

(4) The tested cases of non-tilted when de ≤ 3.0 mm and $\dot{Q}_{Vg} \geq$ 90 L min^{-1}, and tilted when θ ≤ 35°, D ≥ 460 mm, and $\dot{Q}_{Vg} \geq$ 90 L min^{-1}, indicate poor suppression performance by a 0.5 MPa-working pressure water mist, where the normalized lift-up distance of the gas jet $Z_g^* > 1$ and the gas–spray momentum ratio Φ > 1. A few measures to improve the performance of the water mist, i.e., increasing its initial spray momentum, should be taken in leakage incidents where these conditions exist.

Acknowledgment

The authors would like to acknowledge the support by the National Natural Science Foundation of China (NSFC),China (Grant no. 51574210/51874265); the National Key Research & Development Plan of China, China (Grant no. 2018YFC0809502); the Fundamental Research Funds for the Central Universities, China(Grant no.WK2320000039).

References

Adrian, R.J., Westerweel, J., 2011. Particle Image Velocimetry. Cambridge University Press.

Alvarez, R.A., Pacala, S.W., Winebrake, J.J., Chameides, W.L., Hamburg, S.P., 2012. Greater focus needed on methane leakage from natural gas infrastructure. Proc. Natl. Acad. Sci. U. S. A. 109 (17), 6435–6440. https://doi.org/10.1073/pnas.1202407109.

Alvarez, R.A., Zavala-Araiza, D., Lyon, D.R., et al., 2018. Assessment of methane emissions from the U.S. oil and gas supply chain. Science 361, 186–188. https://doi.org/10.1126/science.aar7204.

Broumand, M., Birouk, M., 2016. Liquid jet in a subsonic gaseous crossflow: recent progress and remaining challenges. Prog. Energy Combust. Sci. 57, 1–29. https://doi.org/10.1016/j.pecs. 2016.08.003.

Dong, Y., Gao, H., Zhou, J., Feng, Y., 2002. Evaluation of gas release rate through holes in pipelines. J. Loss Prev. Proc. 15, 423–428. https://doi.org/10.1016/S0950-4230(02)00041-4.

FlowMaster, 2015. Product-Manual for DaVis, 8.3. LaVision GmbH, Gottingen.

Gas Pipeline Incident Data Group, 2014. 9th report of the european gas pipeline incident data group. Period 1970-2013), European. https://www.egig.eu/uploads/bestanden/ba6dfd62- 4044-4a4d-933c-07bf56b82383.

Grant, G.J., Brenton, J., Drysdale, D., 2000. Fire suppression by water sprays. Prog. Energy

Combust. Sci 26 (2), 79–130. https://doi.org/10.1016/S0360-1285(99)00012-X.
Hald, K., Buchlin, J.M., Dandrieux, A., Dusserre, G., 2005. Heavy gas dispersion by water spray curtains: a research methodology. J. Loss Prev. Proc. 18, 506–511. https://doi.org/10.1016/j.jlp.2005.07.026.
Howarth, R.W., Santoro, R., Ingraffea, A., 2011. Methane and the greenhouse-gas footprint of natural gas from shale formations. Clim. Change 106, 679–690. https://doi.org/10.1007/s10584-011-0061-5.
Husted, B.P., 2007. Experimental Measurements of Water Mist Systems and Implications for Modelling in CFD, PhD Thesis. Lund University.
Husted, B.P., Petersson, P., Lund, I., 2009. Comparison of PIV and PDA droplet velocity measurement techniques on two high-pressure water mist nozzles. Fire Saf. J. 44, 1030–1045. https://doi.org/10.1016/j.firesaf.2009.07.003.
Jo, Y.-D., Ahn, B.J., 2003. A simple model for the release rate of hazardous gas from a hole on high-pressure pipelines. J. Hazard Mater. 97, 31–46. https://doi.org/10.1016/S0304-3894(02) 00261-3.
Keane, R.D., Adrian, R.J., 1990. Optimization of particle image velocimeters. I. Double pulsed systems. Meas. Sci. Technol. 1, 1202–1215. https://doi.org/10.1088/0957-0233/1/11/013.
Kuznetsov, G.V., Strizhak, P.A., Volkov, R.S., Vysokomornaya, O.V., 2016. Integral characteristics of water droplet evaporation in high-temperature combustion products of typical flammable liquids using sp and ipi methods. Int. J. Therm. Sci. 108, 218–234. https://doi.org/10.1016/j.ijthermalsci.2016.05.019.
Lelieveld, J., Lechtenböhmer, S., Assonov, S.S., Brenninkmeijer, C.A.M., Dienst, C., Fischedick, M., Hanke, T., 2005. Greenhouse gases: low methane leakage from gas pipelines. Nature 434, 841–842. https://doi.org/10.1038/434841a.
Li, K., Zhou, X., Tu, R., Xie, Q., Yi, J., Jiang, X., 2016. An experimental investigation of supercritical CO2 accidental release from a pressurized pipeline. J. Supercrit. Fluids 107, 298–306. https://doi.org/10.1016/j.supflu.2015.09.024.
Malik, N.A., Dracos, Th, Papantoniou, D.A., 1993. Particle tracking velocimetry in three-dimensional flows. Exp. Fluid 15, 279–294. https://doi.org/10.1007/BF00223406.
Melling, A., 1997. Tracer particles and seeding for particle image velocimetry. Meas. Sci. Technol. 8, 1406–1416. https://doi.org/10.1088/0957-0233/8/12/005.
Murvay, P.S., Silea, I., 2012. A survey on gas leak detection and localization techniques. J. Loss Prev. Proc. 25 (6), 966–973. https://doi.org/0.1016/j.jlp.2012.05.010.
Nam, S., 1996. Development of a computational model simulating the interaction between a fire plume and a sprinkler spray. Fire Saf. J. 26, 1–33. https://doi.org/10.1016/0379-7112(96)00015-X.
National Fire Protection Association (NFPA), 2009. NFPA 59A: Standard for the Production, Storage, and Handling of Liquefied Natural Gas (LNG). NFPA, Quincy, MA.
National Fire Protection Association (NFPA), 2010. NFPA 750: Standard on Water Mist Fire Protection Systems. National Fire Protection Association, Quincy, MA, USA.
Rana, M.A., Cormier, B.R., Suardin, J.A., Zhang, Y., Mannan, M.S., 2008. Experimental study of effective water spray curtain application in dispersing liquefied natural gas vapor clouds. Process Saf. Prog. 27, 345–353. https://doi.org/10.1002/prs.10275.
Rana, M.A., Guo, Y., Mannan, M.S., 2010. Use of water spray curtain to disperse LNG vapor clouds. J. Loss Prev. Proc. 23 (1), 77–88. https://doi.org/10.1016/j.jlp.2009.06.003.
Santangelo, P.E., 2010. Characterization of high-pressure water-mist sprays: experimental analysis of droplet size and dispersion. Exp. Therm. Fluid Sci. 34, 1353–1366. https://doi.org/10.1016/j.expthermflusci.2010.06.008.
Schwille, J.A., Lueptow, R.M., 2006. Effect of a fire plume on suppression spray droplet motion. Atomization Sprays 16, 563-57. https://doi.org/10.1615/AtomizSpr.v16.i5.60.
Strizhak, P.A., Volkov, R.S., 2016. The integral characteristics of the deceleration and entrainment of water droplets by the counter flow of high-temperature combustion products. Exp. Therm. Fluid Sci. 75, 54–65. https://doi.org/10.1016/j.expthermflusci.2016.01.018.
Uzanski, D.T., Buchlin, J.M., 1998. Mitigation of Industrial Hazards by Water Spray Curtains. The fifth conference of the International Emergency Management Society (TIEMS), Washington DC, pp. 19–22.
Volkov, R.S., Kuznetsov, G.V., Strizhak, P.A., 2018. Temperature and velocity fields of the gas-vapor flow near evaporating water droplets. Int. J. Therm. Sci. 134, 337–354. https://doi.org/10.1016/j.ijthermalsci.2018.08.029.
Wang, H., Duncan, I.J., 2014. Likelihood, causes, and consequences of focused leakage and rupture of U.S. natural gas transmission pipelines. J. Loss Prev. Proc. 30, 177–187. https://doi.org/10.1016/j.jlp.2014.05.009.
Wang, X., Liao, G., Qin, J., Fan, W., 2002. Experimental study on the effectiveness of the extinction of a pool fire with water mist. J. Fire Sci. 20, 279–295. https://doi.org/10.1177/073490402762574730.
Wang, Z., Wang, X., Huang, Y., Tao, C., Zhang, H., 2018. Experimental study on fire smoke control using water mist curtain in channel. J. Hazard Mater. 342, 231–241. https://doi.org/10.1016/j.jhazmat.2017.08.026.
Westerweel, J., 2000. Theoretical analysis of the measurement precision in particle image velocimetry. Exp. Fluid 29, S3–S12. https://doi.org/10.1007/s003480070002.
Zhou, Y., Bu, R., Gong, J., Zhang, X., Fan, C., Wang, X., 2018. Assessment of a clean and efficient fire-extinguishing technique: continuous and cycling discharge water mist system. J. Clean. Prod. 182, 682–693. https://doi.org/10.1016/j.jclepro.2018.02.046.
Zhou, Y., Bu, R., Gong, J., Zhang, X., Fan, C., Gong, J., 2019. Performance evaluation of water mist fire suppression: a clean and sustainable fire-fighting technique in mechanically-ventilated place. J. Clean. Prod. 209, 1319–1331. https://doi.org/10.1016/j.jclepro.2018.10.315.
Zhu, P., Wang, X., Li, G., Liu, Y., Kong, X., Huang, Y., Zhao, X., Yuan, J., 2017. Experimental study on interaction of water mist spray with high-velocity gas jet. Fire Saf. J. 93, 60–73. https://doi.org/10.1016/j.firesaf.2017.08.005.